Biosensors and Bioelectronics 71 (2015) 373–379

Contents lists available at ScienceDirect

Biosensors and Bioelectronics

journal homepage: www.elsevier.com/locate/bios

Porphyrinic metal-organic framework as electrochemical probe for DNA sensing via triple-helix molecular switch

Pinghua Ling, Jianping Lei*, Huangxian Ju

State Key Laboratory of Analytical Chemistry for Life Science, School of Chemistry and Chemical Engineering, Nanjing University, Nanjing 210093, PR China

ARTICLE INFO

Article history:
Received 17 February 2015
Received in revised form
14 April 2015
Accepted 17 April 2015
Available online 20 April 2015

Keywords:
Electrochemical sensor
Porphyrin
Metal-organic framework
Triple-helix DNA
Signal amplification

ABSTRACT

An electrochemical DNA sensor was developed based on the electrocatalysis of porphyrinic metal-organic framework (MOF) and triple-helix molecular switch for signal transduction. The streptavidin functionalized zirconium–porphyrin MOF (PCN-222@SA) was prepared as signal nanoprobe via covalent method and demonstrated high electrocatalysis for O_2 reduction. Due to the large steric effect, the designed nanoprobe was blocked for the interaction with the biotin labeled triple-helix immobilized on the surface of glassy carbon electrode. In the presence of target DNA, the assistant DNA in triple-helix will hybridize with target DNA, resulting in the disassembly of triple-helix molecular. Consequently, the end biotin away from the electrode was "activated" for easy access to the signal nanoprobe, PCN-222@SA, on the basis of biotin – streptavidin biorecognition. The introduction of signal nanoprobe to a sensor surface led to a significantly amplified electrocatalytic current towards oxygen reduction. Integrating with DNA recycling amplification of Exonuclease III, the sensitivity of the biosensor was improved significantly with detection limit of 0.29 fM. Moreover, the present method has been successfully applied to detect DNA in complex serum matrix. This porphyrinic MOF-based strategy has promising application in the determination of various analytes for signal transduction and has great potential in bioassays.

1. Introduction

Metal-organic frameworks (MOFs), a new class of crystalline porous materials with fascinating structures and intriguing properties, have attracted a great deal of research interest for their potential applications, especially in gas storage and separation, catalysis, drug delivery and sensing (Hu et al., 2014; Lan et al., 2009; O'Keeffe and Yaghi, 2012; Perry et al., 2009; Pramanik et al., 2011; Wang et al., 2012, 2014). Their pore space and functionality can be easily regulated by direct encapsulation of the functional molecules into the cavities of MOFs (Chen et al., 2012; Larsen et al., 2011), postsynthetic modification (Cohen, 2012), and ligand design (Das et al., 2011; Suh et al., 2012; Umemura et al., 2011; Zhu et al., 2012). In particular, design of specific ligands in the frame becomes popular methods for giving MOFs various functionalities. Interestingly, porphyrin that is the active centre of natural enzymes can be readily functionalized as struts for the construction of MOFs (Alkordi et al., 2008; Farha et al., 2011; Fateeva et al. 2012; Zou et al., 2012). These MOFs can mimic natural enzymes with high catalytic activity, substrate selectivity as well as water/chemical stability (Feng et al., 2012, 2013). Therefore, it is a promising way to design an efficient signal transduction platform by utilizing the catalytic activity of porphyrinic MOFs in biosensing, especially for DNA detection.

DNA is the most important genetic material of living beings, and many methods have been exploited to detection of DNA. Among the detection methods for DNA, the electrochemical method has many advantages such as high sensitivity, low-cost, simplicity and portability (Fan et al., 2003; Farjami et al., 2011; Xiao et al., 2007). For signal amplification, many materials have been involved such as enzymes (Liu et al., 2015; Xuan et al., 2013), conjugated polymer (Gaylord et al., 2005), and nanoparticles (Wang et al., 2010). Exonuclease III (Exo III) is a nuclease that selectively catalyzes the stepwise hydrolysis of mononucleotides from the blunt or the recessed 3′-hydroxyl termini of duplex DNA without the requirement of specific recognition sequences (Shevelev and Hubscher, 2002). Exo III-assisted signal amplification strategy was proposed as a useful electrochemical aptasensor for the detection of DNA and Hg^{2+} (Xuan et al., 2013; Zhao et al., 2014). On the other hand, there are various DNA structures for signal transduction such as nucleic acid walker (Tian et al., 2005), Hairpin DNA (Huang et al., 2014; Wu et al., 2009), tetrahedron (Pei et al., 2012), triple-helix DNA (Gao et al., 2014) and scissor (Elbaz et al., 2012). For example, Tan and co-worker have designed a new type of aptamer-based sensing platform using a triple-helix DNA (Zheng et al., 2011). Mao and co-workers have proposed a DNA

* Corresponding author.
E-mail address: jpl@nju.edu.cn (J. Lei).

http://dx.doi.org/10.1016/j.bios.2015.04.046
0956-5663/

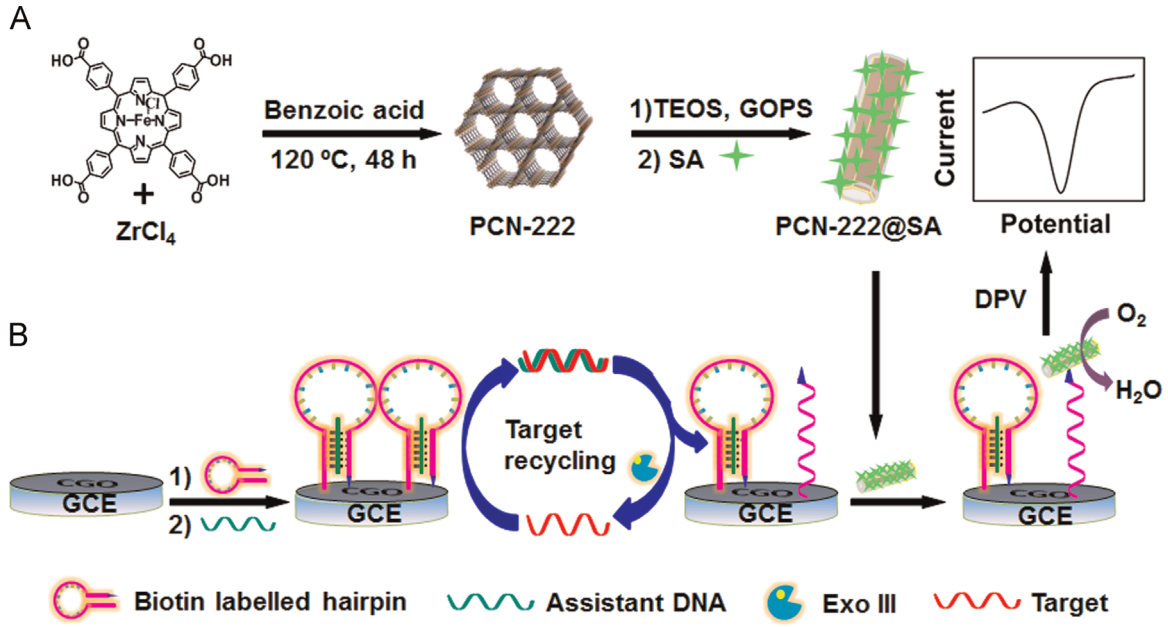

Scheme 1. (A) Synthesis of PCN-222@SA composite, and (B) electrochemical strategy coupling with target recycling amplification for DNA sensing.

nanomachine based on duplex–triplex transition triggered by the changes in the solution pH value (Chen et al., 2004). Therefore, the DNA structure switch provides an efficient way for construction of DNA signal transduction platform in bioanalysis.

In this work, coupling with electrocatalysis of PCN-222 as signal nanoprobe and Exo III signal amplification, an electrochemical DNA sensor was designed for DNA detection through the structure switch of triple-helix DNA (Scheme 1). The signal nanoprobe PCN-222, was synthesized using porphyrin as linker and functionalized with streptavidin (SA) as recognition element. The sensing platform was prepared by immobilizing triple-helix DNA labeled with biotin at 5' end on a glassy carbon electrode (GCE) modified with graphene. Due to the large steric effect, the hairpin DNA was expected to be in the "closed" state of triple-helix DNA, in which the nanoprobe was blocked for the interaction with the immobilized biotin end. In the presence of target DNA, its recognition with assistant DNA triggers the Exo III cleavage process, accompanied with the target recycling and the release of the hairpin DNA. Afterward, the introduction of PCN-222@SA nanoprobe to the sensor surface led to a significantly amplified electrocatalytic current towards oxygen reduction. The porphyrinic MOF-based sensor with enhanced current is easily used to detect DNA with a detection limit of 0.29 fM, and shows a great potential in complex samples. The porphyrinic MOF-based strategy has great potential application in signal transduction and monitoring the important biomolecules in biological system.

2. Materials and methods

2.1. Materials and reagents

Zirconium chloride ($ZrCl_4$), benzoic acid, ethanol, dimethylformamide (DMF), polyvinylpyrrolidone (PVP, MW 40k), (3-glycidyloxypropyl) trimethoxysilane ($C_9H_{20}O_5Si$, GOPS), streptavidin, 1-(3-dimethylaminopropyl)-3-ethylcarbodiimide hydrochloride (EDC, ≥98%), tetramethoxysilane (TEOS), and N-Hydroxysuccinimide (NHS) were purchased from Sigma-Aldrich Inc (USA). Iron(III) meso-5,10,15,20-tetrakis(4-carboxyphenyl)porphyrin chloride (FeTCPP) was obtained J&K Scientific Ltd. (China). Ammonium hydroxide (25 wt%) and toluene were purchased from Nanjing Chemical Reagent Co., LTD (China). Carboxylic graphene oxide (CGO, purity >99.8%, carboxyl ratio >5.0 wt%, single layer ratio >80%) was purchased from Nanjing XFNano Materials Tech Co. Ltd. (Nanjing, China). Exo III was obtained from New England Biolabs Ltd. (Shanghai, MA, USA). In our work, 10 mM PBS containing 20 mM NaCl, 2.5 mM $MgCl_2$ (pH 8.0) was used as oligonucleotide stock solution and washing solution. Exo III digestion buffer was prepared with 50 mM PBS, 200 mM NaCl and 2.5 mM $MgCl_2$ with 20 units Exo III. The hybridization solutions with various pH values were prepared by mixing stock standard solutions of 10 mM sodium phosphate buffer containing 20 mM KCl and 2.5 mM $MgCl_2$, and then adjusted to the required pH value with 0.1 M HCl or NaOH. All reagents were of analytical grade and without further purification. Millipore Milli-Q water (≥18.2 MΩ cm) was used for the experiments throughout. Human serum samples were generously provided by Jiangsu Province Tumor Hospital. All DNA oligonucleotides were synthesized by Sangon Inc. (Shanghai, China). The sequences of DNA oligonucleotides are given below:

Hairpin DNA (HpDNA): 5′-biotin-*CTCTCT*CGGTTGGTGTGGTTGG *CTCTCT*CAAAAA AAAAA-NH_2-3′

Hairpin DNA 1 (Hp1): 5′-biotin-*CTCTCTCT*GGTTGGTGTGGTTG G*TCTCTCT*CAAAAAA AAAA- NH_2-3′

Hairpin DNA 2 (Hp2): 5′-biotin-*CTCTCT*GGTTGGTGTGGTTG G*TCTCT*CAAAAAAAA AA-NH_2-3′

Hairpin DNA 3 (Hp3): 5′-biotin-*CTCT*CGGTTGGTGTGGTT GG*CTCT*CAAAAAAAAAA -NH_2-3′

Assistant DNA (aDNA): 5′-GAGAGAGAGATATA-3′

Target DNA (tDNA): 5′-TATATCTCTCTCTCAAAAA-3′

The italic letters represent the arm sequences.

2.2. Apparatus

The scanning electron microscope (SEM) images were obtained from an S-4800 scanning electron microscope (Hitachi, Japan). X-ray diffraction (XRD) was determined through a Cu sealed tube (λ=1.54178 Å) at 40 kV and 40 mA to found the crystal structures of the MOF. UV–vis spectra were recorded on UV-3600 UV–vis–NIR spectrophotometer (Shimadzu Co., Kyoto, Japan). The nitrogen isotherm of PCN-222 was obtained on the Micromeritics ASAP2020 at 77 K. The infrared spectra were observed on a Vector

22 Fourier transform infrared spectrometer (Bruker Optics, Germany). Circular dichroism (CD) spectra were measured on a chirascan circular dichroism chromatograph (Applied Photophysics LTD, England). The 10% native polyacrylamide gel electrophoresis (PAGE) was performed with 5 × Tris–Borate–EDTA (TBE) buffer. The loading sample was prepared by mixing 7 μL of DNA sample, 1.5 μL 6 × loading buffer with 1.5 μL UltraPower dye, and kept for 3 min so that the dye could integrate with DNA completely. The gel was run at 90 V for 90 min in 1 × TBE buffer, and then scanned with Molecular Imager Gel Doc XR (BIO-RAD, USA). Electrochemical experiments, including cyclic voltammetry (CV) and differential pulse voltammograms (DPV), were conducted on CHI 660D electrochemical workstation (Shanghai CH Instruments, China) with a three-electrode system including glassy carbon electrode (GCE), saturated calomel electrode (SCE) and platinum wire as working, reference and counter electrodes, respectively.

2.3. Synthesis of PCN-222

The PCN-222 was obtained according to reported method previously (Feng et al., 2012). Typically, 70 mg of $ZrCl_4$, 50 mg of FeTCPP and 2700 mg of benzoic acid were dissolved in 8 mL DMF ultrasonically. Then the mixture solution was filled into 25 mL Teflon liner, placed in autoclave and heated at 120 °C for 48 h. After cooling to room temperature, the dark brown needle-shaped crystal was obtained via centrifugation and washed with DMF. In order to obtain the highly dispersible PCN-222, the PVP as the stabilizer was added to obtain the PVP coated PCN-222 (Graf et al., 2003; Rodríguez-Lorenzo et al., 2011).

2.4. Preparation of epoxy-functionalized PCN-222

Prior to epoxy-functionalization, the PCN-222 was treated with TEOS to get the SiO_2 coated PCN-222 composite (Taylor-Pashow et al., 2009). Then 1 mg of SiO_2 coated PCN-222 was added into 100 μL of 5% GOPS (v/v) in dry toluene and stirred for 12 h at room temperature. Afterward, the synthesized epoxy-functionalized PCN-222 was washed with toluene and ethanol solution, sequentially. The composite was dried and activated in an oven at 80 °C for 1 h under N_2 atmosphere.

2.5. Bioconjugation of PCN-222 with SA

PCN-222@SA was prepared via the conjugation between NH_2 groups of SA and epoxy groups on the PCN-222. Typically, 200 μL SA (2 mg mL^{-1}) was injected into 500 μL of the epoxy-functionalized PCN-222 aqueous solution (1 mg mL^{-1}). The mixture was slightly stirred at 4 °C for 12 h to make the NH_2 groups conjugate to epoxy groups. After washed with 0.1 M PBS (pH 7.4) at 10,000 rpm for 10 min to remove the unbound SA, the PCN-222@SA was re-dispersed in 0.1 M PBS (pH 7.4) and stored at 4 °C for further use.

2.6. Construction and electrochemical detection of biosensor

Prior to usage, the GCEs were polished with a slurry of alumina oxide powder (1.0 and 0.05 μm) on chamois leather, washed ultrasonically and dried at room temperature. 1 mg CGO was dispersed in 1 mL of water by sonication for 60 min. Then 3 μL of CGO suspension (1 mg mL^{-1}) was dropped on the GCE surface and dried in air, and 20 μL of 400 mM EDC and 100 mM NHS were cast onto the GCE surface for 30 min. After washed, the electrode was exposed to 1 μM hairpin DNA in 10 mM PBS buffer (pH 8.0) containing 20 mM NaCl and 2.5 mM $MgCl_2$ for 4 h. The hairpin DNA modified electrode was then incubated with assistant DNA at pH 6.2 for 60 min. After formation of the triple-helix, target DNA and Exo III were dropped on the electrode under 37 °C for 2 h. Finally, the electrode was immersed in the solution of PCN-222@SA (1.0 mg mL^{-1}). The biosensor was utilized for electrochemical measurements with CV and DPV (a pulse amplitude of 50 mV and a width of 50 ms) in 0.1 M pH 7.4 oxygen-saturated PBS.

3. Results and discussion

3.1. Characterization of PCN-222

The PCN-222 was synthesized by using FeTCPP as linker and Zr as node via solvothermal reaction. The SEM images of PCN-222 showed that PCN-222 particles adopt a needle-shaped single crystal with several μm in length (Fig. 1A). The surface of PCN-222 is clearly visible with hexahedron geometry (inset in Fig. 1A). The XRD pattern revealed that the PCN-222 crystalizes in space group *P6/mmm* (Feng et al., 2012), and the subtle difference was due to a small amount of impurities in the original sample (Fig. S1). The obtained materials of PCN-222 were further characterized using FT-IR spectroscopy (Fig. S2), in which exhibits characteristic peaks for big ring skeleton absorptions at 1710 (w), 1659 (s), 1558 (s), 1416 (vs), the O–H stretch at 1000 (s), and benzene rings at 871 (w) and 780 (m) cm^{-1} in FeTCPP, respectively. The permanent porosity of PCN-222 and the pore size were examined by N_2 sorption experiments at 77 K (Fig. 1B), which revealed a typical type IV isotherm (Ferey et al., 2005) and a Brunauer–Emmett–Teller surface area of 1050 $m^2\ g^{-1}$. The isotherm of PCN-222 exhibits a steep increase at the point of P/P_o=0.3, suggesting the mesoporosity. The experimental total pore volume was

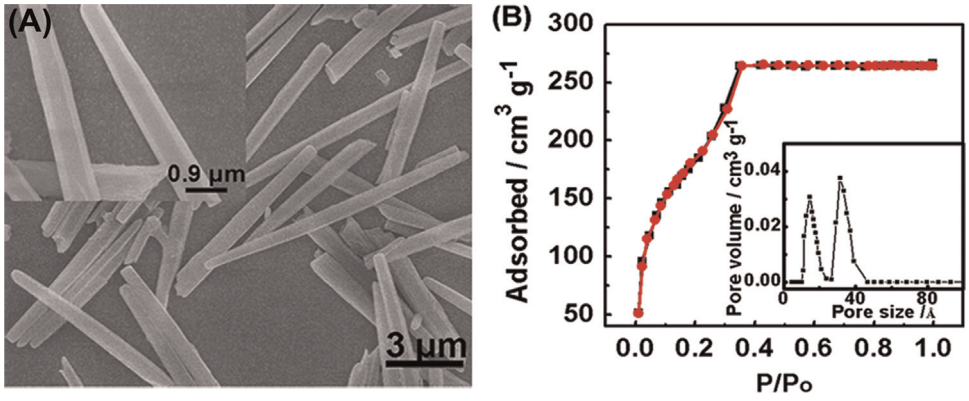

Fig. 1. (A) SEM image of PCN-222 at different scales. Inset: Enlarged PCN-222 morphology and (B) N_2 adsorption isotherm of PCN-222. Inset: DFT pore size distribution with N_2 at 77 K.

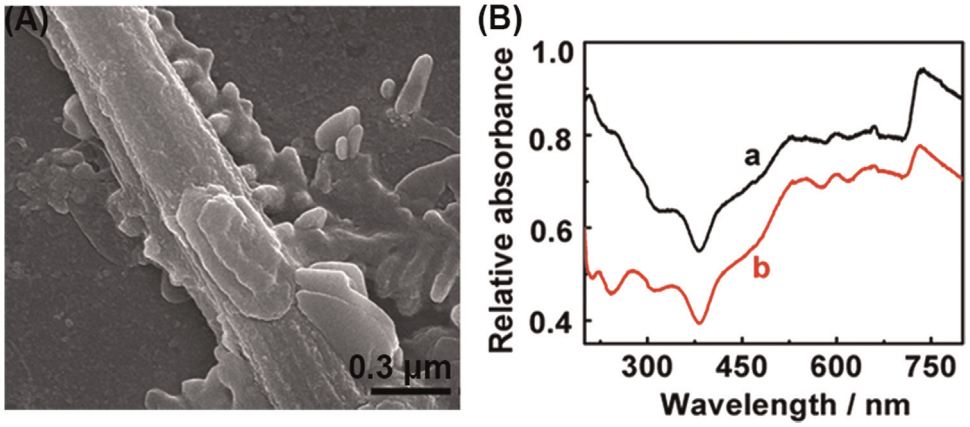

Fig. 2. (A) SEM image of PCN-222@SA. (B) UV–vis absorption spectra of PCN-222 (a), and PCN-222@SA (b).

1.24 $cm^3\ g^{-1}$. From inset in Fig. 1B, two types of pores are observed with sizes of 1.3 nm and 3.2 nm via the density functional theory (DFT), assigned to triangular microchannels and hexagonal mesochannels, respectively. Such high surface areas should be attributed to the 3-D open channels in the framework, which is beneficial to construct the catalytic interface.

3.2. Characterization of PCN-222@SA

The SEM image of PCN-222@SA showed that the morphology and structure of the nanoparticles were maintained and the surface of these nanoparticles became rough after modifying with SA (Fig. 2A), indicating SA could be linked to the surface of PCN-222. To further verify the formation of the functional MOFs, UV–vis absorption spectrometry was used to investigate the fabricated process of the nanoprobe (Fig. 2B). After PCN-222 was modified with SA, a 278 nm absorption peak was observed in comparison with that of pure PCN-222, suggesting that SA could be bound to PCN-222 surface.

3.3. Electrocatalytic behavior of PCN-222

The CVs of different electrodes were measured in pH 7.4 oxygen-saturated PBS at 5 μL of PCN-222 (0.1 mg mL^{-1}) and 5 μL of PCN-222@SA (0.1 mg mL^{-1}) modified GCE (Fig. 3A). Comparing with PCN-222/GCE in N_2-saturated PBS (curve a), the PCN-222/GCE showed clearly reduction peaks at around −0.28 V in O_2-saturated PBS, which is corresponding to the electrochemical reduction of oxygen (curve b). When the PCN-222@SA was immobilized on the GCE (curve c), the current response is slightly smaller than that of PCN-222/GCE (curve b) due to the SA protein hindered access to catalytic sites.

3.4. Feasibility of electrochemical DNA biosensor

The feasibility of the electrochemical DNA biosensor was investigated in Fig. 3B. When the HpDNA probes were immobilized on the GCE, the sensor showed a large peak current at around −0.28 V (curve a). Upon the addition of aDNA, the peak current decreased to 15% (curve b). This phenomenon implied that the aDNA was hybridized with the HpDNA probes to form the triple-helix to block the binding with signal nanoprobe. In the presence of tDNA, the peak current increased (curve c). The tDNA was hybridized with the aDNA, and then the HpDNA probes could bind with PCN-222@SA to catalyze towards O_2 reduction as detectable electrochemical signal. When the Exo III was further introduced, the peak current increased after Exo III treatment for target recycling (curve d). As control, Exo III has no effect to the triple-helix in the absence of target (curve e). In addition, when using PCN-222 as signal nanoprobe, the catalytic current in the presence of tDNA is similar to the blank, indicating the low nonspecific binding. These results showed that this biosensor is highly specific recognition in the detection of DNA.

From CD spectrum (Fig. S3), the HpDNA (curve a) and aDNA

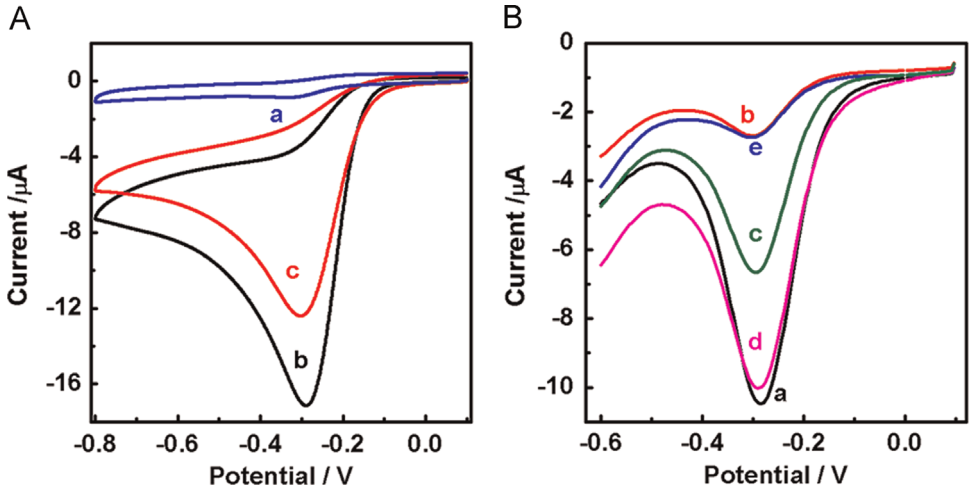

Fig. 3. (A) CVs of PCN-222 (0.1 mg mL^{-1}) modified GCE in 0.1 M N_2-saturated PBS (a), PCN-222 (0.1 mg mL^{-1}) modified GCE (b) and PCN-222@SA (0.1 mg mL^{-1}) modified GCE (c) in 0.1 M O_2-saturated PBS. Scan rate: 50 mV s^{-1}. (B) DPV responses of the biosensor to HpDNA (a), (a) + aDNA (b), (b) + tDNA (c), (c) + Exo III (d) and (b) + Exo III (e) in 0.1 M O_2-saturated PBS.

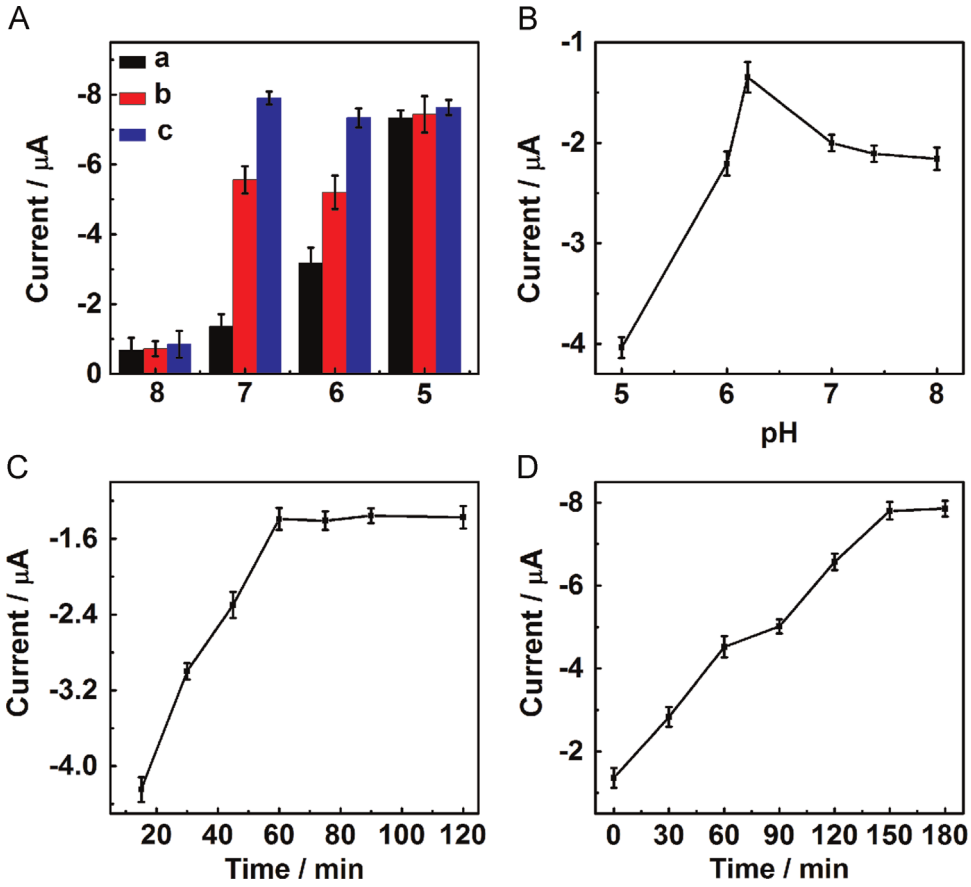

Fig. 4. Effects of (A) number of bases in the arm of hairpin DNA, a, b and c represent the responses of the biosensor to aDNA + HpDNA, aDNA + HpDNA + tDNA and aDNA + HpDNA + tDNA + Exo III, respectively, (B) pH and (C) hybridization time between HpDNA and aDNA in the absence of tDNA, and (D) enzyme digestion time on electrochemical response.

(curve b) had two positive bands at 280 nm and 220 nm. After hybridized, the spectrum (curve c) has two negative bands at 246 nm and 212 nm, and a positive band at 280 nm. The characteristic peak at 212 nm indicates the triple-stranded DNA formation (Plum and Breslauer, 1995; Soto et al., 2002). To ensure the hybridization of HpDNA and aDNA, the PAGEs were shown in Fig. S4. Compared to the respective duplex and single strand (lanes a–d), triple-helix DNA molecules (lane e) could be observed to migrate slower. After Exo III treatment, a new product band with a fast migration speed was observed (lanes g and h), which should be contributed to a cleavage product of Exo III towards the formed double stranded DNA of aDNA–tDNA. Meanwhile, the band of triple-helix was observed in lane i, suggesting that Exo III did not affect the triple-helix.

3.5. Optimization of detection conditions

In order to achieve high sensitivity, experimental conditions such as the arm length of HpDNA, pH, the incubation time for formation of triple-helix and the cleavage time of Exo III were optimized in Fig. 4. Because the stability of triple-helix structure depends on the arm length of HpDNA (Dohno et al., 2002), the different arm sequences were designed in this system. When the arm length increased to 8 bases (Fig. 4A), the triple-helix could not be disassembled even in the presence of high concentration of target. Decreasing the arm sequence length of the HpDNA to 6 or 5 bases, the current changed slightly since triple-helix was not formed. As a result, the arm length of 7 bases is required for optimal target probe design and application to generate the large signal change.

The pH values of PBS are the key role during the procedure of triple-helix formation because the stability of the Hoogsteen base pairing is pH dependent (Vasquez and Glazer, 2002). When the pH value was increased, the current reached to the minimum at pH 6.2 and then increased (Fig. 4B), indicating the high stability of triple-helix. Therefore, pH 6.2 was selected for further studies in the subsequent experiments. As the time of forming triple-helix was prolonged, the currents decreased as shown in Fig. 4C. Upon incubation time of more than 60 min, the signal of current reached a plateau, indicating that the reaction may complete in 60 min. Therefore, 60 min was chosen as the optimization of incubation time in the experiments. In order to optimize the enzyme digestion time, a series of experiments were carried out with different time (Fig. 4D). The currents increased rapidly with time between 0 and 150 min and showed a leveling off after 150 min. Ultimately, a hybridization time of 60 min and enzyme digestion time of 150 min were chosen as the optimal experimental conditions.

3.6. Detection of target DNA

To ensure the present electrochemical DNA biosensor can be used for sensitive quantification of target DNA, the current responses induced by different concentrations of target DNA were evaluated with DPV measurements in 0.1 M pH 7.4 PBS. Under the optimized conditions, the results showed that electrochemical signal increased with the increasing of target DNA (Fig. 5A). With higher target DNA concentration, more assistant DNA on the electrode were cleaved, resulting in that more HpDNA probes could bind with PCN-222@SA to electrocatalytic reduction of O_2. Moreover, the peak current displayed a good linear relationship

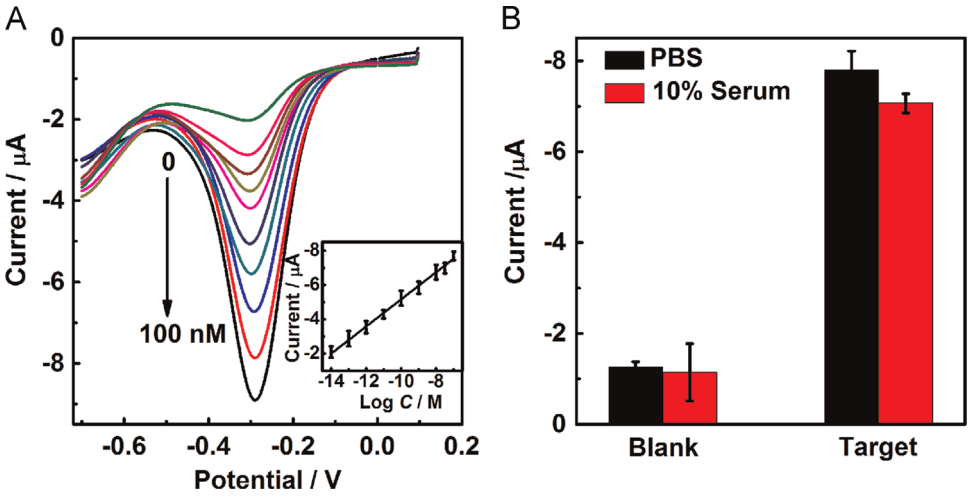

Fig. 5. (A) DPV responses of the biosensor to different concentrations of target DNA at 0, 10 fM, 100 fM, 1 pM, 10 pM, 100 pM, 1 nM, 10 nM, 50 nM and 100 nM (from top to down). Inset: calibration curve of current intensity vs. logarithmic value of DNA concentration. (B) Practicality test of the sensor in buffer and 10% serum solution in the presence and absence 100 nM target DNA.

with the concentration of target DNA in the range from 10 fM to 100 nM (inset in Fig. 5A). The detection limit was 0.29 fM at the S/N =3, which was lower than that of target-induced strand displacement strategy using methylene blue as electrochemical indicator (400 fM) (Xiao et al., 2006) and the enzyme-amplification electrochemical DNA biosensor (10 fM) (Liu et al., 2008). This high sensitivity of DNA biosensor is due to the nicking endonuclease signal amplification and good electrocatalytic activity of porphyrinic MOF.

The repeatability of the biosensor was examined at the target DNA concentrations of 50 fM, 50 pM and 20 nM. The relative standard deviations (RSD) for six measurements were 2.5%, 4.3% and 3.1%, respectively, thus giving good repeatability. In addition, ten independently prepared electrodes were used with the RSD of 3.6%, thereby indicating good fabrication reproducibility. Although the biosensor can be used once, it will be a simple and low-cost by using a screen-printed carbon as working electrode.

3.7. Application in human serum sample

To exclude the potential interfering species, we examined the DPV response of the biosensor in PBS containing 0.5 mM uric acid (UA) and 0.1 mM ascorbic acid (AA). In comparison with PBS, the DPV current in UA and AA solution exhibited the decrease of 4.0% and 1.6%, respectively (Fig. S5), indicating the high anti-interference of this method. To demonstrate the practicability of the proposed strategy in complex matrices, standard target DNA solution (100 nM) was spiked into 10% diluted human serum samples and tested by the sensor (Fig. 5B). The current response obtained in serum samples was slightly lower than that obtained in PBS. The recoveries were calculated to be 95.0 ± 1.5% (n=3) which indicated that the DNA sensor had excellent practicality for target DNA with porphyrinic MOF as electrochemical probe.

4. Conclusions

This work developed a highly sensitive electrochemical DNA sensor by integrating the electrocatalysis of porphyrinic MOF with a triple-helix molecular switch for signal transduction. The dual functionalized MOF probe was prepared with porphyrin as electrocatalytic active site and SA as recognition element via covalent method. Significantly, the designed porphyrinic MOF composite demonstrated high electrocatalysis for O_2 reduction in neutral solution, which benefits in electrochemical DNA sensing. Upon target-triggered triple-helix molecular switch, the signal nanoprobe was introduced to a sensor surface via SA–biotin recognition system, and led to a significantly amplified electrocatalytic current for signal readout. With the aid of Exo III recycling amplification, the "turn-on" strategy was achieved for DNA detection with 7-order magnitude linear range and detection limit down to sub femtomolar level. Also, the unique structure of triple-helix DNA provides a universal platform for highly specific detection of DNA. The porphyrinic MOF-based platform and strategy offer not only an excellent signal transduction for detecting a wide range of the analysts but also are easy in design of the integrated signal amplification in trace detection.

Acknowledgments

We gratefully acknowledge the National Natural Science Foundation of China (21375060, 21135002 and 21121091) and Priority development areas of the National Research Foundation for the Doctoral Program of Higher Education of China (20130091130005).

Appendix A. Supplementary Information

Supplementary data associated with this article can be found in the online version at 10.1016/j.bios.2015.04.046.

References

Alkordi, M.H., Liu, Y., Larsen, R.W., Eubank, J.F., Eddaoudi, M., 2008. J. Am. Chem. Soc. 130, 12639–12641.
Chen, Y., Lee, S.H., Mao, C.D., 2004. Angew. Chem. Int. Ed. 43, 5335–5338.
Chen, Y., Lykourinou, V., Vetromile, C., Hoang, T., Ming, L.J., Larsen, R., Ma, S.Q., 2012. J. Am. Chem. Soc. 134, 13188–13191.
Cohen, S.M., 2012. Chem. Rev. 112, 970–1000.
Das, M.C., Xiang, S.C., Zhang, Z.J., Chen, B.L., 2011. Angew. Chem. Int. Ed. 50, 10510–10520.
Dohno, C., Nakatani, K., Saito, I., 2002. J. Am. Chem. Soc. 124, 14580–14585.
Elbaz, J., Wang, F., Remacle, F., Willner, I., 2012. Nano Lett. 12, 6049–6054.
Fan, C.H., Plaxco, K.W., Heeger, A., 2003. Proc. Natl. Acad. Sci. USA 100, 9134–9137.
Farha, O.K., Shultz, A.M., Sarjeant, A.A., Nguyen, S.T., Hupp, J.T., 2011. J. Am. Chem. Soc. 133, 5652–5655.
Farjami, E., Clima, L., Gothelf, K., Ferapontova, E.E., 2011. Anal. Chem. 83, 1594–1602.
Fateeva, A., Chater, P.A., Ireland, C.P., Tahir, A.A., Khimyak, Y.Z., Wiper, P.V., Darwent,

J.R., Rosseinsky, M.J., 2012. Angew. Chem. Int. Ed. 51, 7440–7444.
Feng, D.W., Chung, W.C., Wei, Z.W., Gu, Z.Y., Jiang, H.L., Chen, Y.P., Darensbourg, D.J., Zhou, H.C., 2013. J. Am. Chem. Soc. 135, 17105–17110.
Feng, D.W., Gu, Z.Y., Li, J.R., Jiang, H.L., Wei, Z.W., Zhou, H.C., 2012. Angew. Chem. Int. Ed. 51, 10307–10310.
Ferey, G., Mellot-Draznieks, C., Serre, C., Millange, F., Dutour, J., Surblé, S., Margiolaki, I., 2005. Science 309, 2040–2042.
Gao, W., Zhang, L., Zhang, Y.M., Liang, R.P., Qiu, J.D., 2014. J. Phys. Chem. C 118, 14410–14417.
Gaylord, B.S., Massie, M.R., Feinstein, S.C., Bazan, G.C., 2005. Proc. Natl. Acad. Sci. USA 102, 34–39.
Graf, C., Vossen, D.L.J., Imhof, A., van Blaaderen, A., 2003. Langmuir 19, 6693–6700.
Huang, Y., Wen, W., Du, D., Zhang, X.H., Wang, S.F., Lin, Y.H., 2014. Biosens. Bioelectron. 61, 598–604.
Hu, Z.C., Deibert, B.J., Li, J., 2014. Chem. Soc. Rev. 43, 5815–5840.
Lan, A.J., Li, K.H., Wu, H.H., Olson, D.H., Emge, T.J., Ki, W., Hong, M.C., Li, J., 2009. Angew. Chem. Int. Ed. 48, 2334–2338.
Larsen, R.W., Wojtas, L., Perman, J., Musselman, R.L., Zaworotko, M.J., Vetromile, C. M., 2011. J. Am. Chem. Soc. 133, 10356–10359.
Liu, G., Wan, Y., Gau, V., Zhang, J., Wang, L.H., Song, S.P., Fan, C.H., 2008. J. Am. Chem. Soc. 130, 6820–6825.
Liu, S.F., Cheng, C.B., Liu, T., Wang, L., Gong, H.W., Li, F., 2015. Biosens. Bioelectron. 63, 99–104.
O'Keeffe, M., Yaghi, O.M., 2012. Chem. Rev. 112, 675–702.
Pei, H., Liang, L., Yao, G.B., Li, J., Huang, Q., Fan, C.H., 2012. Angew. Chem. Int. Ed. 51, 9020–9024.
Perry, J.J., Perman, J.A., Zaworotko, M.J., 2009. Chem. Soc. Rev. 38, 1400–1417.
Plum, G.E., Breslauer, K.J., 1995. J. Mol. Biol. 248, 679–695.
Pramanik, S., Zheng, C., Zhang, X., Emge, T.J., Li, J., 2011. J. Am. Chem. Soc. 133, 4153–4155.
Rodríguez-Lorenzo, L., Rica, R.D.L., Álvarez-Puebla, R.A., Liz-Marzán, L.M., Stevens, M.M., 2011. Nat. Mater. 11, 604–607.
Shevelev, I.V., Hubscher, U., 2002. Nat. Rev. Mol. Cell Biol. 3, 1–12.
Suh, M.P., Park, H.J., Prasad, T.K., Lim, D.W., 2012. Chem. Rev. 112, 782–835.
Soto, A.M., Loo, J., Marky, L.A., 2002. J. Am. Chem. Soc. 124, 14355–14363.
Tian, Y., He, Y., Chen, Y., Yin, P., Mao, C.D., 2005. Angew. Chem. Int. Ed. 44, 4355–4358.
Taylor-Pashow, K.M.L., Rocca, J.D., Xie, Z.G., Tran, S., Lin, W.B., 2009. J. Am. Chem. Soc. 131, 14261–14263.
Umemura, A., Diring, S., Furukawa, S., Uehara, H., Tsuruoka, T., Kitagawa, S., 2011. J. Am. Chem. Soc 133, 15506–15513.
Vasquez, K.M., Glazer, P.M., 2002. Q. Rev. Biophys. 35, 89–107.
Wang, Y.S., Liu, B., Mikhailovsky, A., Bazan, G.C., 2010. Adv. Mater. 22, 656–659.
Wang, C., Zhang, T., Lin, W.B., 2012. Chem. Rev. 112, 1084–1104.
Wang, X.S., Chrzanowski, M., Yuan, D.Q., Sweeting, B.S., Ma, S.Q., 2014. Chem. Mater. 26, 1639–1644.
Wu, Z.S., Zheng, F., Shen, G.L., Yu, R.Q., 2009. Biomaterials 30, 2950–2955.
Xiao, Y., Lubin, A.A., Baker, B.R., Plaxco, K.W., Heeger, A.J., 2006. Proc. Natl. Acad. Sci. USA 103, 16677–16680.
Xiao, Y., Qu, X.G., Plaxco, W.K., Heeger, J.A., 2007. J. Am. Chem. Soc. 129, 11896–11897.
Xuan, F., Luo, X.T., Hsing, I.M., 2013. Anal. Chem. 85, 4586–4593.
Zhao, J., Hu, S.S., Zhong, W.D., Wu, J.G., Shen, Z.M., Chen, Z., Li, G.X., 2014. ACS Appl. Mater. Interfaces 6, 7070–7075.
Zheng, J., Li, J.S., Jiang, Y., Jin, J.Y., Wang, K.M., Yang, R.H., Tan, W.H., 2011. Anal. Chem. 83, 6586–6592.
Zhu, C.F., Yuan, G.Z., Chen, X., Yang, Z.W., Cui, Y., 2012. J. Am. Chem. Soc. 134, 8058–8061.
Zou, C., Zhang, Z.J., Xu, X., Gong, Q.H., Li, J., Wu, C.D., 2012. J. Am. Chem. Soc. 134, 87–90.